# Novel Frequency-Domain Inertia Mapping and Estimation in Power Systems using Wavelet Analysis

Mohamed Abouyehia, Agusti Egea-Alvarez, Member, IEEE, Sumeet S. Aphale, Senior Member, IEEE, Khaled H. Ahmed, Senior Member, IEEE

***Abstract*— In recent power systems, accurately estimating system inertia is crucial for stability, especially with the increased integration of renewable energy sources. This paper proposes a novel wavelet-based method for estimating the inertia of synchronous machines and the dynamic inertia of converter-interfaced generators (CIG). The proposed method estimates the inertia constant in the frequency domain, contrasting traditional time domain methods. The proposed method capitalises on the unique capability of wavelet transform coefficients to analyse rapid changes in active power and frequency signals. The magnitude of these coefficients is then utilised to measure the strength of the transit periods on those signals, which serves as an indicator of the power system's inertia constant. This paper also derives a novel mathematical relationship between frequency-domain inertia estimates and their time-domain equivalents. The proposed method is scalable, demonstrating efficiency across both small and large power systems. Control hardware-in-the-loop (CHiL) simulations are employed using a real-time, high-speed piecewise linear electrical circuit simulator (PLECS) alongside a digital signal processor (DSP) to validate the proposed method. The results reveal that the proposed method offers superior stability and demonstrates resilience against system noise, as well as potential numerical issues common in traditional methods.**

***Index Terms*— Inertia estimation, regional system inertia, wavelet transform, equivalent inertia, frequency stability.**

## I. INTRODUCTION

The rapid integration of CIGs in modern power systems, driven by the increasing adoption of renewable energy sources, has fundamentally altered the dynamics of system inertia. In contrast to the traditional synchronous generators (SGs) that inherently provide rotational inertia, CIGs typically lack this natural stabilising characteristic [1]. Therefore, this shift from SGs to CIGs presents significant challenges for grid stability and resilience [2]. Consequently, inertia estimation in power systems, especially those dominated by CIGs, has become important for several reasons [3]. For instance, inertia estimation enables precise assessment of the grid capacity to withstand frequency fluctuations. Furthermore, it supports optimal resource allocation and operational planning in mixed generator environments. Finally, it informs the design and implementation of advanced control schemes for virtual inertia provision by CIGs.

Over recent decades, inertia estimation has evolved significantly, including a wide range of methods [4, 5]. These methods can be broadly categorised into three main groups: traditional swing equation-based methods [6], data-driven methods [4], and frequency domain-based estimation methods. Each category offers unique advantages and faces distinct challenges in addressing the complexities of power systems.

Traditional swing equation-based methods form the foundation of inertia estimation. These methods rely on the fundamental relationship between active power and frequency changes during system disturbances. The swing equation links these parameters through the inertia constant, providing a direct means of estimation. Within this category, three primary methods have emerged: 1) The rate of change of frequency (RoCoF) method, which calculates the inertia by dividing power imbalance by frequency change rate. RoCoF offers quick insights for inertia constant but struggles with numerical issues at low-rate changes [6, 7]. 2) The polynomial fitting method, which addresses the RoCoF limitations by fitting polynomials to frequency response for often more accurate, numerically stable results. However, it poses computational challenges and delays [8]. 3) The sliding window method involves real-time estimation by averaging sequential data rather than relying on a single measurement. Although, it enhances real-time tracking and accuracy, the method precision depends on the window size, system dynamics, and data quality [9]. Overall, the traditional swing equation-based methods are simple and offer direct physical interpretation, however, they often struggle with numerical stability and sensitivity to measurement noise. Moreover, these methods also require significant disturbances in frequency and active power signals for inertia assessment [4].

In response to the limitations of swing equation-based methods, researchers have developed various data-driven methods. These data-driven estimation methods use advanced computational algorithms to extract inertia estimates from system measurements. Within this category, four primary methods have emerged: 1) Artificial intelligence (AI) methods, such as artificial neural networks (ANN), which utilize historical data to provide real-time inertia estimates [10]. However, these methods require large datasets, risk overfitting, and are seen as "black boxes". 2) The sparse identification of nonlinear dynamics (SINDy) method, which is commonly used for complex grid inertia estimation. This method uses linear regression to match parameters with observed data [11]. It needs accurate data but is flexible and efficient [12, 13]. 3) Auto regressive, moving average, and exogenous (ARMAX)

[1]M. Abouyehia is with department of Electronic and Electrical Engineering, Strathclyde University, Glasgow, G1 1XQ, UK and is also with department of Engineering Mathematics and Physics, Faculty of Engineering, Alexandria University, Alexandria 21544, Egypt (e-mail: mohamed.aboyehia@strath.ac.uk, mohamed.abuyehia@alexu.edu.eg).

Khaled H. Ahmed and Agusti Egea-Alvarez are with department of Electronic and Electrical Engineering, Strathclyde University, Glasgow, G1 1XQ, UK (e-mail: khaled.ahmed@strath.ac.uk; agusti.egea@strath.ac.uk).

Sumeet S. Aphale is with the Artificial Intelligence, Robotics and Mechatronic Systems (ARMS) Group, School of Engineering, University of Aberdeen, AB24 3UE Aberdeen, U.K. (e-mail: s.aphale@abdn.ac.uk).

method, which is another system identification method. It creates accurate models from input-output data. Its success depends on the data quality and model tuning. Moreover, it needs advanced computation and extensive data [14]. 4) Kalman filter-based methods [15] are designed to deduce the state of dynamic systems in the presence of noise. Kalman methods depend on inherent assumptions and limitations. Therefore, any deviations in the system actual behaviour from the assumed model can result in inaccuracies. Overall, the data-driven based method offer improved performance in complex, non-linear systems, however, they often require extensive datasets and significant computational resources.

The third category of inertia estimation methods operates in the frequency domain, contrasting with the time-domain focus of traditional and most data-driven methods. In the frequency domain-based estimation methods, Fourier transform is used to transform the swing equation from time domain to frequency domain. By doing so, these methods can capture the bandwidth of electromechanical oscillations more effectively. Overall, these methods enhances precision, numerical stability, and making estimation more efficient. However, they require extensive computational time and faces limitation such as signal noise and complexity in large power systems [7, 16].

Despite the advancements in each of these categories, significant challenges remain in inertia estimation. This gap underscores the need for a reliable, resilient, efficient, and robust estimation method. Therefore, this paper proposes a novel wavelet transform (WT)-based inertia estimation method. The proposed method utilises the frequency measurements in conjunction with the measured active power, and then analysing their wavelet coefficients to detect and evaluate transients. Furthermore, a new frequency inertia index is derived from these wavelet coefficients, which provides an indicative measure of the power system inertia in the frequency domain. Finally, the relation between the inertia derived in frequency domain and the actual inertia in the time domain is derived. The key contributions of this paper include the conceptualization of a novel WT-based approach for inertia estimation and the mathematical derivation of the relationship between inertia index in the frequency domain and the actual time domain inertia. The proposed wavelet transform-based method offers several advantages over existing inertia estimation methods. For example, it ensures numerical stability by avoiding derivative calculations and potential zero divisions. The method efficiency scales favourably with network expansion due to its reliance on only two measurement signals: frequency and active power. Moreover, it demonstrates superior computational efficiency by eliminating the need for training processes or regression techniques common in data-driven methods. Lastly, the inherent noise-resistant properties of wavelet transforms enhance the method's robustness against signal disturbances.

The structure of the paper is organised as follows. Section II reviews the basic concepts of the WT. Section III outlines the proposed inertia estimation method and its mathematical derivation. Section IV presents the controller hardware-in-the-loop results using PLECS and includes a comparative analysis with other estimation methods. Section V presents a sensitivity analysis to validate the capabilities of the proposed method.

## II. Wavelet Transform

The wavelet transform is a mathematical method which can be used for detecting the transient events [17]. In contrast to traditional Fourier methods, which provide only a frequency spectrum (time information is ignored), the WT captures information in both time and frequency domains. This dual representation is particularly useful for analysing non-stationary signals, where frequency components evolve over time as in transient events [18]. The WT mainly localise and categorise the transient periods using elementary functions called wavelets. The process involves convolving the electrical signal with that wavelet function, sliding it over the signal to compare their similarity at different points in time. When the wavelet aligns closely with a transient event, it produces a high convolution value, identifying the event exact location. The wavelet function provides two key adjustable parameters: translation and scale. The translation enables the wavelet to slide across the signal during convolutions, while adjusting the scale allows the wavelet function to be stretched or compressed. Using wavelets of different scales, one can zoom in for a detailed look or zoom out to capture wider transient features.

The WT is represented mathematically as:

$$WT_{f(t)}(a,b) = \int_{-\infty}^{\infty} f(t)\,\psi^{c}\left(\frac{t-b}{a}\right)dt \qquad (1)$$

where, $f(t)$ denotes the target signal being analysed. $\psi(t)$ is the selected wavelet function. The superscript symbol (c) typically represents the complex conjugate operation. The use of the complex conjugate is fundamental for conserving signal energy and accurately representing the frequency characteristics. The scale $(a)$ adjusts the wavelet size. A scale above one stretches the wavelet, highlighting the signal low-frequency components, while a scale between zero and one compresses it, highlighting the high-frequency components. Meanwhile, the translation $(b)$ moves the wavelet through the signal, ensuring comprehensive coverage. $WT_{f(t)}(a,b)$ represents the wavelet coefficient of $f(t)$ at scale $a$ and position $b$. The magnitude of these coefficients is subsequently employed to localise and identify transients.

There are different types of wavelet functions $\psi(t)$, which can be classified into either complex or real functions, as depicted in Fig. 1. Real wavelets, such as Mexican Hat, Morlet, and Double Gaussian, provide only amplitude information. Thus,

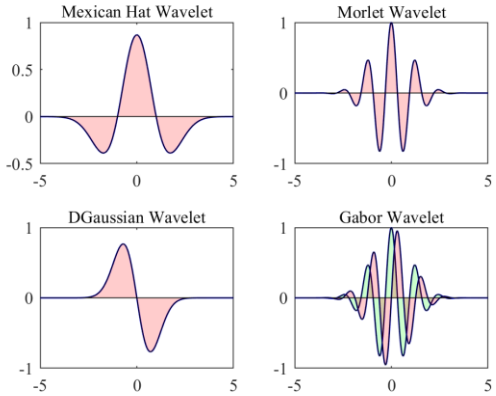


**Fig. 1.** Different types of wavelet functions $\psi(t)$.

the real wavelets are more straight forward and often preferred for tasks like edge detection or singularities identification. On the other hand, complex wavelets such as the Gabor, offer both amplitude and phase information. Therefore, complex wavelets are suitable for applications, where oscillatory patterns are of interest. In this context, when focusing on transient detection, complex wavelets are typically preferred. Their capability to capture phase information facilitates accurate timing and a richer representation of transient events.

Fig. 2 shows the capabilities of the WT in transient detection as an example. This example utilises a general unit step function $u(t)$ to represent the transient events. As shown in Fig. 2(a), $u(t)$ has an initial magnitude of 4. Then it faces two major transient events: firstly, at 0.3 s, where it decreases from 4 to 3, marking a transient strength of 1; subsequently, at 0.6 s, it faces a further reduction from 3 to 1, signifying a transient strength of 2 double the intensity of the initial transient. Subsequently, this signal $u(t)$ is analysed using WT in (1) and the complex Gabor wavelet function. The absolute values of the resulting wavelet coefficients $|WT_{u(t)}(a,b)|$ is shown in Fig. 2(b). There are two notable peaks in the wavelet domain, corresponding precisely to the times 0.3 s and 0.6 s in Fig. 2(b). Thereby highlighting the wavelet ability in localising transient events in time. Furthermore, the magnitudes of these peaks are directly proportional to the transient strengths in the time domain with the coefficient at 0.6 s (0.334) being twice as intense as its counterpart at 0.3 s (0.167). This denotes the efficiency of wavelet coefficients not only in detecting but also in quantifying transient strength. The WT key advantage is avoiding reliance on derivative terms to determine the strength of the transients. Instead, it emphasises frequency representation, proving to be both clear and stable even with noise. This aspect will be explored further in the following sections.

## III. Proposed Wavelet Transform Based Inertia Estimation Method

This section introduces a novel inertia constant ($H$) estimation method using the coefficients of WT. The inertia constant plays a crucial role in determining the acceleration or deceleration of the rotor angle in response to sudden changes in active power

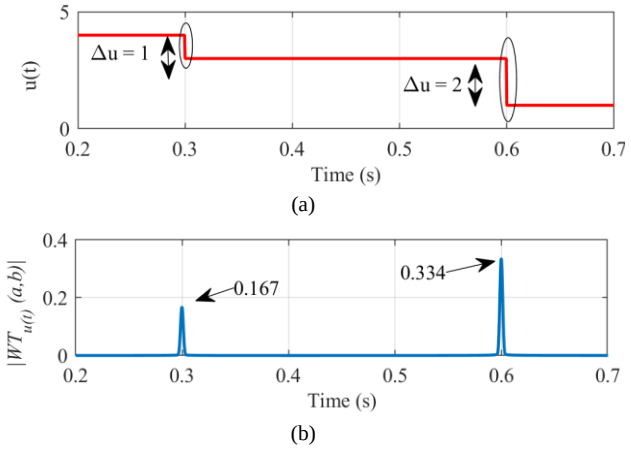


**Fig. 2.** Demonstrating the wavelet transform efficiency in transient detection. (a) General step function highlighting transient events and (b) wavelet coefficients magnitude reflecting transient strengths.

of machines. Its importance is highlighted in the transfer function described as follows [19]:

$$\frac{2HZ}{\omega_0}\frac{d^2\delta}{dt^2} = \Delta P \tag{2}$$

where, $\frac{d^2\delta}{dt^2}$ stands for the acceleration of rotor angle $\delta$ over time, which effectively demonstrates the speed at which the angle changes due to disturbances. $\Delta P$ signifies the change in the output active power. $Z$ is the volt-ampere ($VA$) base and $\omega_0$ is the rated (base) angular speed of the rotor. Additionally, the relationship between the rotor angle and the angular speed of the rotor can be represented as:

$$\frac{d^2\delta}{dt^2} = \omega_0 \frac{d\overline{\Delta\omega_r}}{dt} \tag{3}$$

where, $\omega_r$ denotes the angular speed of the rotor. By substituting (3) into (2), the following equation is derived:

$$2H\frac{d\overline{\Delta\omega_r}}{dt} = \overline{\Delta \mathrm{P}} \tag{4}$$

It is worth mentioning that (4) is written in per unit values with respect to $Z$ and $\omega_0$, as shown in Fig. 3, where the bar notation indicates that the quantity is in per unit value. One key observation is that the inertia constant is determined during the transient periods; therefore, equation (4) can be reformulated as follows:

$$H_t = \frac{\int_{t_1}^{t_1+\Delta t} \overline{\Delta p}\, dt}{2\overline{\Delta\omega_r}} \tag{5}$$

where, $t_1$ is the instance when the transient occurs, while $\Delta t$ specifies the transient period.

The formulation of inertia constant in (5) is straightforward. However, the process of directly integrating in the time domain poses challenges, notably in the precise identification of the transient duration ($\Delta t$) and the accurate determination of the transient strength concerning both active power and angular velocity. Consequently, these parameters are evaluated within the frequency domain by utilising the coefficients of WT in (1). The following subsections depend on (1) and (5) to propose a novel frequency inertia index and its equivalent mapping in the time domain.

### A. New Simplified Frequency Inertia Index

This section presents a new simple frequency inertia index. For simplicity, equation (5) is refined by excluding the integration term and the factor 0.5. As a result, the inertia constant can be simply represented in the time domain using the following ratio (assuming a very small transient period $\Delta t$ and utilising only the power change ΔP instead of its integral):

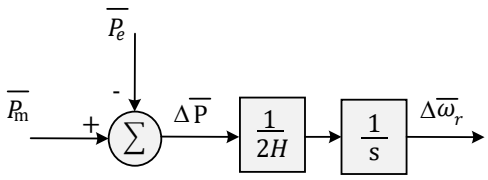


**Fig. 3.** Transfer function loop for the inertia constant.

$$H_t = \frac{\overline{\Delta p}}{\Delta \omega_r} \tag{6}$$

The subscript '$t$' in $H$ is introduced to specify that this value is derived from the time domain analysis. As described in Section II, the transient variations in active power $\overline{\Delta p}$ and angular frequency $\overline{\Delta \omega_r}$ can be precisely identified through the maximal coefficients of the WT in (1). Therefore, the measurement of $\bar{p}(t)$ and $\bar{\omega}_r(t)$ are collected. Subsequently, WT in (1) is applied separately for $\bar{p}(t)$ and $\bar{\omega}_r(t)$ as follows:

$$\mathcal{WT}_{\mathrm{p(t)}}(a,b) = \sqrt{\frac{2}{\pi}} \int_{-\infty}^{\infty} \bar{p}(t)\, e^{i\omega_0\left(\frac{t-b}{a}\right)} e^{\frac{-\left(\frac{t-b}{a}\right)^2}{2}} dt \tag{7}$$

$$\mathcal{WT}_{\omega(t)}(a,b) = \sqrt{\frac{2}{\pi}} \int_{-\infty}^{\infty} \bar{\omega}_r(t)\, e^{i\omega_0\left(\frac{t-b}{a}\right)} e^{\frac{-\left(\frac{t-b}{a}\right)^2}{2}} dt \tag{8}$$

As previously highlighted, the complex Gabor function is the optimal wavelet function for transient detection. Consequently, the wavelet function $\psi(t)$ in (1) is replaced with the Gabor expression $\left(\sqrt{\frac{2}{\pi}} e^{-i\omega_0\left(\frac{t-b}{a}\right)} e^{\frac{-\left(\frac{t-b}{a}\right)^2}{2}}\right)$. Where, $\omega_0$ is the non-dimensional frequency and is considered to be 6 to satisfy the admissibility condition [20]. Upon examination of the coefficients from the WT presented in equations (7) and (8), detailed frequency spectrums for both active power and angular speed are derived. The strength of the transients in the signals, represented as $\overline{\Delta \mathrm{P}}$ and $\overline{\Delta \omega_r}$, is determined by the maximum absolute value of the coefficients from equations (7) and (8), respectively. These maximum coefficients are denoted as $\max_{a,b}\left|\mathcal{W}_{\mathrm{p(t)}}(a,b)\right|$ and $\max_{a,b}\left|\mathcal{W}_{\omega(\mathrm{t})}(a,b)\right|$. Based on these findings, the inertia index can be estimated in the frequency domain using the following ratio:

$$H_f = \frac{\max_{a,b}\left|\mathcal{W}_{\mathrm{p(t)}}(a,b)\right|}{\max_{a,b}\left|\mathcal{W}_{\omega(\mathrm{t})}(a,b)\right|} \tag{9}$$

where, the subscript '$f$' in $H$ is introduced to specify that this value is derived from the frequency domain analysis. One key observation is that $H_f$ does not exactly equate the actual inertia $H$ due to the omission of the integral action and the factor 0.5 in (5). However, it can be claimed that $H_f$ precisely maps the behavior of $H_t$. To validate this claim, the transfer function, depicted in Fig. 3, is simulated in MATLAB for different values of $H_t$. The process starts with introducing a step change in $\overline{\Delta \mathrm{P}}$, which is achieved by adjusting the value of $\bar{P}_e$ from 1 pu to 0.5 pu (it is noteworthy that any specific step change value can be used). The consequential effect on the angular speed $\overline{\omega_r}$ is measured. Subsequently, both signal $\bar{p}_e$ and $\overline{\omega_r}$(t) are processed through the WT, as outlined in (7) and (8). Then, the peak wavelet coefficients for the input active power $\left(\max_{a,b}\left|\mathcal{W}_{\mathrm{p(t)}}(a,b)\right|\right)$ and output angular frequency $\left(\max_{a,b}\left|\mathcal{W}_{\omega(\mathrm{t})}(a,b)\right|\right)$ are determined from the frequency spectrum. Finally, the $H_f$ is calculated using these maximum values as in (9). The simulation results for different values of $H_t$ are presented in Table I.

TABLE I. COMPARISON ANALYSIS BETWEEN $H_t$ AND THE NEW FREQUENCY INERTIA INDEX $H_f$.

| Exact value ($H_t$) | $\max_{a,b}\left\|\mathcal{W}_{\mathrm{p(t)}}\right\|$ | $\max_{a,b}\left\|\mathcal{W}_{\omega(\mathrm{t})}\right\|$ | Estimated $H_f$ | $\frac{H_t}{H_f}$ |
|---|---|---|---|---|
| 0.1 | 3.17 | 1.9574e-03 | 1.6195e+03 | 6.1747e-05 |
| 1 | 3.17 | 1.9574e-04 | 1.6195e+04 | 6.1747e-05 |
| 5 | 3.17 | 3.9149e-05 | 8.0973e+04 | 6.1749e-05 |
| 10 | 3.17 | 1.9574e-05 | 1.6195e+05 | 6.1747e-05 |
| 100 | 3.17 | 1.9574e-06 | 1.6195e+06 | 6.1747e-05 |

Table I provides insightful remarks on the relation between $H_t$ and $H_f$, which are summarised as follows; 1) $H_t$ and $H_f$ have a consistent proportional relationship. If $H_t$ changes by a certain factor, $H_f$ will be changed also by the same factor. 2) The integral action and the factor (0.5) in the time domain translates to a scalar multiplication in the frequency domain by a specific value (≈6.17e-05). The following subsection will prove that this value is equal to $\frac{2(\Delta t)^2}{\pi}$, where $\Delta t$ is the transient period that is determined by WT in the frequency domain. Notably, this relation represents one of the pivotal contributions of this paper. 3) The estimated value of $H_f$ remains constant regardless the magnitude of step changes introduced to the input signal $\bar{P}_e$. This behaviour mirrors that of the actual value of $H_t$, which should not be dependent on transient strength. Therefore, it can be claimed that the newly developed frequency inertia index ($H_f$) effectively reflects the exact inertia in the time ($H_t$).

### *B. Mathematical Relationship Between Frequency Inertia Index and Time Domain Inertia Value*

In the previous analysis, the WT of $\overline{\Delta p}$ was considered instead of its integration $\int_{t_1}^{t_1+\Delta t} \overline{\Delta p}\, dt$. The results produced the formula of the frequency inertia index in (9). Now, the focus shifts to the full formulation: $\int_{t_1}^{t_1+\Delta t} \overline{\Delta p}\, dt$ instead of $\overline{\Delta p}$. Define the integral over the transient period as:

$$y(t) = \int_{t_1}^{t_1+\Delta t} \overline{\Delta p}\, dt \tag{10}$$

Therefore, the WT of $y(t)$ using Gabor wavelet with standard $a$ and $b$, is defined as:

$$\mathcal{WT}_{\int \mathrm{p(t)}(a,b)} = \sqrt{\frac{2}{\pi}} \int_{-\infty}^{\infty} \left( \underbrace{\int_{t_1}^{t_1+\Delta t} \overline{\Delta p}\, dt}_{y(t)} \right) e^{-\frac{t^2}{2}} e^{i\omega_0 t} dt \tag{11}$$

For simplicity, the integral term in y(t) can be expressed in terms of a convolution operation. The integral essentially computes the area under the curve $\overline{\Delta p}(t)$ from $t_1$ to $t_1 + \Delta t$, and the convolution of two functions is a measure of the overlap between the two functions as one function slide over the other. Therefore, if a convolution operation is performed between $\overline{\Delta p}(t)$ and a rectangular pulse of width $\Delta t$ (specially $rect_{\Delta t}(t)$), the result would be equivalent to integrating $\overline{\Delta p}(t)$ over a moving window of width ($\Delta t$). Therefore, $y(t)$ can be further represented as follows:

$$y(t) = \int_{t_1}^{t_1+\Delta t} \overline{\Delta p}\, dt \equiv \overline{\Delta p}(t) * rect_{\Delta t}(t) \tag{12}$$

where, "$*$" denotes the convolution operation and $rect_{\Delta t}(t)$ is a rectangular pulse function of width size $\Delta t$. This rectangular pulse is mathematically defined as follows:

$$rect_{\Delta t}(t) = \begin{cases} 1 & |t| \le 0.5\ \Delta t \\ 0 & OTHERWISE \end{cases} \tag{13}$$

It is worth mentioning that the formula in (12) is valid if $rect_{\Delta t}(t)$ aligns with the transient of $\overline{\Delta p}(t)$ at time $t_1$ during the convolution. The proposed WT-based inertia estimation method depends on identifying the maximum frequency component within the frequency domain at the transient instance. This necessitates concentrating on the frequency components of $rect_{\Delta t}(t)$ precisely at time $t_1$. For simplicity, the frequency components of the standard rectangular function with a unit width and unit height ($rect(t)$) are determined using the Fourier transform. Then based on these findings, the frequency components of the scaled and shifted pulse rectangular ($rect_{\Delta t}\ (t)$) can be derived for WT as follows:

$$\mathcal{F}\big(rect(t)\big) = \text{sinc}(\pi f) \tag{14}$$

where, sinc(πf) is the Sine Cardinal function and is defined as the ratio $\frac{\sin(\pi f)}{\pi f}$. To exactly match the transient period, it is essential to scale this function by Δt and introduce a shift by $t_1$. This modification can be mathematically articulated based on the scale and time-shift properties of the Fourier transform:

$$\mathcal{F}\big(rect_{\Delta t}(t-t_1)\big) = \frac{\sin(\pi f \Delta t)}{\pi f} e^{j2\pi f t_1} \tag{15}$$

The formula in (15) describes the frequency components of the scaled and shifted pulse rectangular, ($rect_{\Delta t}(t-t_1)$). However, the proposed method concentrates on the term $\max_{a,b}\left|\mathcal{W}_{rect(t)}(a,b)\right|$, which identifies the frequency component offering the most significant contribution in the rectangular pulse using WT. Consequently, the expression in (15) necessitates modification to align with the estimation derived from the WT. Generally speaking, the WT can be considered as a variant of the Fourier transform, modulated by a damping factor ($e^{-\frac{t^2}{2}}$) that occurs across various time intervals and scales. Therefore, it is crucial to examine the impact of this damping term on the rectangular function presented in (15). Using the same previous concept in (12), the damping term in the integration formula of the WT can be interpreted as a convolution process. By analysing this damping term in the frequency domain, it translates to:

$$\mathcal{F}\big(Damp_{WT}(t)\big) = \ 2e^{-\frac{(2\pi f-\omega_0)^2}{2}} \tag{16}$$

where, $Damp_{WT}(t)$ is the damping of the WT. When scaling this damping by $\Delta t$ to align with the rectangular function, the transformation produces:

$$\mathcal{F}\left(Damp_{WT}\left(\frac{t}{\Delta t}\right)\right) = \ 2\Delta t\ e^{-\frac{(2\pi\Delta t\, f-\omega_0)^2}{2}} \tag{17}$$

Therefore, the frequency spectrum of the rectangular function, when modulated by the damping term, can be computed by multiplying the results from (15) and (17) as follows:

$$\begin{aligned}&\mathcal{F}\left(Damp_{WT}\left(\frac{t}{\Delta t}\right) * rect_{\Delta t}(t-t_1)\right)\\ &= 2\Delta t\ e^{-\frac{(2\pi\Delta t\, f-\omega_0)^2}{2}}\ \frac{\sin(\pi f\Delta t)}{\pi f} e^{j2\pi f t_1}\\ &= \frac{2\Delta t}{\pi f}\sin(\pi f\Delta t)\, e^{-\frac{(2\pi f\Delta t-\omega_0)^2}{2}}\ e^{j2\pi f t_1}\end{aligned} \tag{18}$$

The frequency component offering the most significant contribution in the rectangular pulse using WT, $\max_{a,b}\left|\mathcal{W}_{rect(t)}(a,b)\right|$, is equivalent to the maximum frequency contribution from (18) . As shown in (18) the maximum is given by $2\Delta t/\pi f$ . This peak occurs at $f = 1/2\Delta t$ where the sine wave is equals one. Consequently, the $\max_{a,b}\left|\mathcal{W}_{rect(t)}(a,b)\right|$ will equal to $(4(\Delta t)\text{^}2)/\pi$.

The final relation between $H_f$ and $H_t$is described as follows:

$$\begin{aligned}H_t = \frac{\int_{t_1}^{t_1+\Delta t}\overline{\Delta p}\ dt}{2\overline{\Delta\omega_r}} &= \frac{\max_{a,b}\left|\mathcal{W}_{\text{p(t)}}(a,b)\right| \times \frac{4(\Delta t)^2}{\pi}}{2\times\max_{a,b}\left|\mathcal{W}_{\omega(t)}(a,b)\right|}\\ &= H_f \times \frac{2(\Delta t)^2}{\pi}\end{aligned} \tag{19}$$

The value of Δt is precisely determined from the WT.

### *C. Proposed Inertia Estimation Method*

This section presents the proposed inertia estimation method using the wavelet transform, grounded on the previous mathematical derivation in (19). The proposed inertia estimation method can be employed to estimate the inertia of a single machine within a standalone network or multiple machines within interconnected, multi-area power systems.

#### 1) Proposed Inertia Estimation Method for Standalone Single-Machine Network

This part outlines the proposed inertia estimation method for a single machine in a standalone network. The steps of the proposed estimation method are shown in Fig. 4, and can be summarised as follows: i) The algorithm begins with the construction of the wavelet function, $\psi(t)$ with various scales a. Various wavelet functions can be utilised. However, the Gabor wavelet is highly efficient for analysing transient periods. ii) Active power $\left(\bar{p}(t)\right)$ and angular frequency $\left(\bar{\omega}(t)\right)$ are then measured at the machine bus. iii) These measurements are analysed using the wavelet transform, as specified in equations (7) and (8). This analysis involves convolving the measured signals, angular frequency and active power with the selected wavelet function $\psi(t)$ across different scales ($a$). This means the wavelet function $\psi(t)$, at various sizes (scales), is slid over $f(t)$, and at each position, a multiplication and convolution are performed. This convolution results in wavelet coefficients that capture the signal time and frequency domain characteristics at that scale and position. Each scale of the wavelet function $\psi(t)$ matches a specific frequency, allowing the WT coefficients to show those frequencies presence at different times within the input signal. iv) By evaluating the WT coefficients magnitude and locating peaks or areas of high magnitude, transients in $\bar{p}(t)$ and $\bar{\omega}(t)$ are accurately detected and localised. The magnitude representation of the coefficients during a transient appears as a bell-shaped curve, as shown in Fig. 4.

The strength of the transient event is directly proportional to the maximum of the wavelet coefficients in the transient period. Larger coefficients suggest a stronger transient event. To achieve greater accuracy, the proposed method considers not

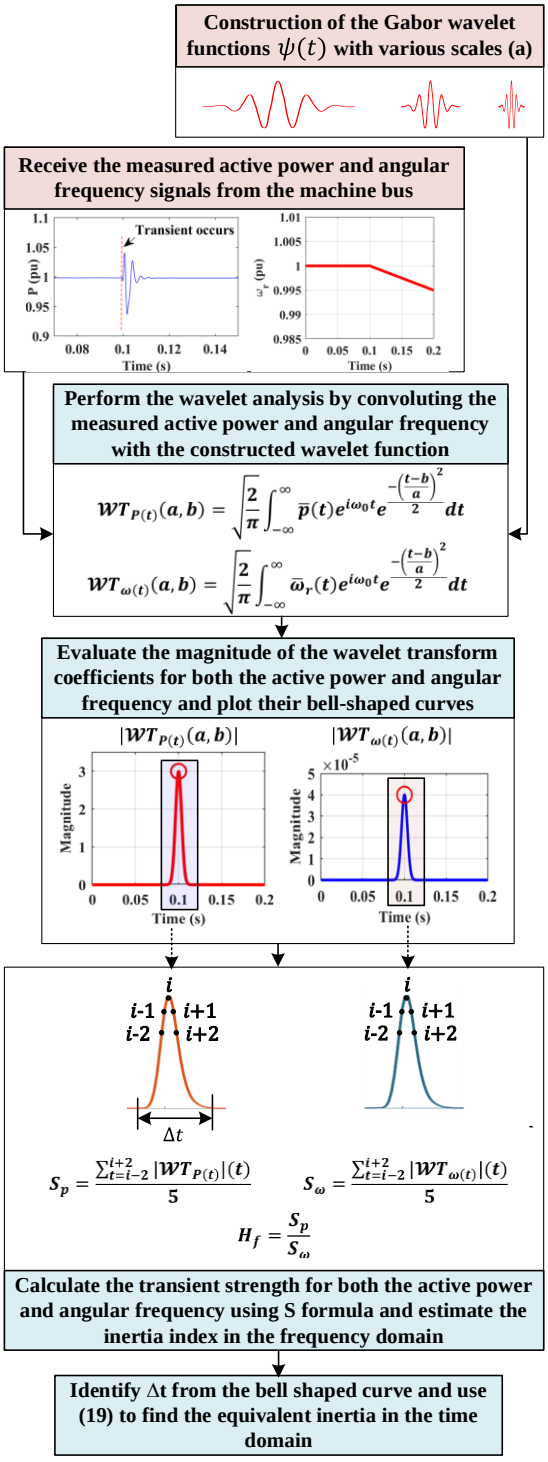


**Fig. 4**. Transient detection and strength measurement by wavelet coefficient analysis.

just the peak value to identify the transient strength but also an average including several points around the peak. For simplicity, this typically involves 4 samples (2 before and 2 after the peak). Consequently, an accurate measurement of the transient event strength, denoted as $S$, is calculated. This is done by averaging the absolute values of the selected points in the transient region, leading to the formula $S = \frac{\sum_{t=i-2}^{t=i+2}|WT_{f(t)}|(t)}{5}$, where $i$ is the peak index of the bell curve. This value of $S$ provides a measure of the transient event overall energy or strength for any signal $f(t)$. v) At the standalone machine bus associated with either the synchronous generator or CIGs, the strength coefficient ($S$) is calculated twice. The first calculation refers to the active power measurement, denoted as $S_p$, and the second refers to the angular frequency signal, denoted as $S_\omega$. The frequency inertia index, $H_f$ is then calculated by the ratio $S_p/S_\omega$. This ratio offers valuable insight into the inertia characteristics of the synchronous machine or the CIGs. vi) The duration of the transient period (Δt) is simply identified in the frequency domain by measuring the width of the bell-shaped curve depicted in Fig. 4. Finally, the frequency domain inertia index $H_f$ is correlated to its corresponding value in the time domain $H_t$ using (19).

2) Proposed Inertia Estimation Method for Interconnected Multi-Area Networks

This part outlines the proposed inertia estimation method for serval machines in interconnected multi-area networks. A key feature of the proposed inertia estimation method is its enhanced efficiency as the network grows. This efficiency stems from its reliance on only two measurement signals: angular frequency and active power. Fig. 5 provides a general representation of the proposed inertia estimation method in a multi-area power system, aimed at identifying the inertia constants across different areas of the network. Initially, as shown in Fig. 5, the phasor measurement unit (PMU), which is strategically placed at each area bus, gathers the data relating to angular frequency and active power. These data from different areas within the power system are collected. Post-collection, the proposed inertia estimation method is employed to identify

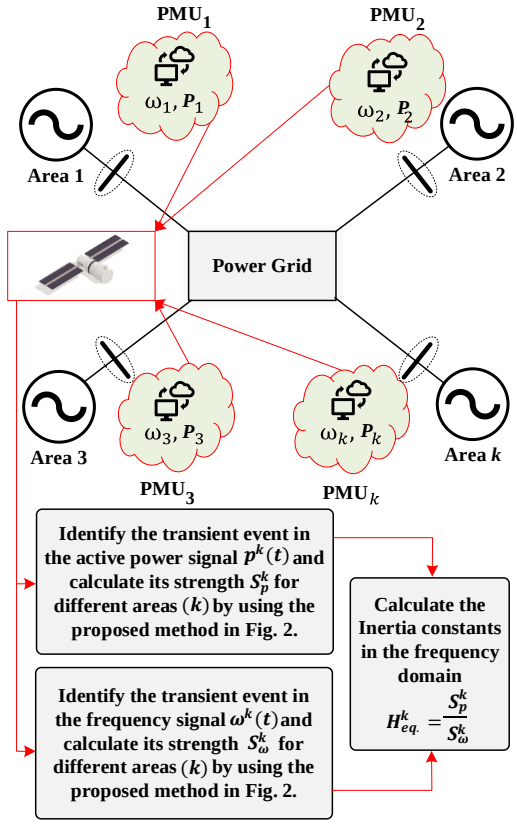


**Fig. 5.** Proposed inertia estimation method for a multi-area power system using wavelet transform.

transients within both the active power and frequency signals using (7) and (8). With the WT coefficients as an analytical tool, the proposed inertia estimation method identifies the transient strength in the active power and frequency signals for every individual area. Furthermore, the method yields a notable ratio $\frac{S_p^k}{S_\omega^k} \times \frac{2(\Delta t)^2}{\pi}$, which serves as a representative of the equivalent inertia in the time domain, where k indicates the area number in the power system.

## IV. Control Hardware in the Loop Validation

To validate the proposed inertia estimation method, the inertia of the standard IEEE 9 bus system is estimated for two case studies. The IEEE 9 bus system is depicted in Fig. 6, with its parameters are detailed in Table II. The standard IEEE 9 bus system consists of three interconnected areas with three synchronous generators; however, the generator at area 3 is replaced with a CIG, as shown in Fig. 6. With this network, a comprehensive assessment of the proposed method compatibility with both traditional synchronous generators and non-synchronous converters is carried out. The system-level components, including transformers, generators, transmission lines, loads, and buses, are implemented within the PLECS platform for real-time simulation, as depicted in Fig. 7. The proposed inertia estimation method is executed on a 150 MHz DSP labelled as (TMS320F28335ZJZA). The real-time platform operates on 4 cores based on ARM Cortex-A53 processor at 1.5 GHz. This simulation provides the active power and angular frequency measurements at the terminals of three areas: bus 1, bus 2, and bus 3. These signals are then transmitted to the inertia estimation method on the DSP. The inertia estimation method analyses the active power and frequency signals from the three areas, measures transients, and subsequently identifies the inertia of each area, as in section III. Finally, the output results derived from the proposed method will be compared against the actual inertia of these three areas.

### A. Case Study 1

This case study assumes that the three areas have identical inertia of value 3.7 s. To assess the inertia response, a 40 MW load is applied to bus 9 at 0.1 s by closing the switch (S1) in Fig. 6. Comparing the step 40 MW load value to the load values in Table II, this step is smaller, highlighting the method effectiveness with small transients. Fig. 8(a) shows the angular frequency data measured from the three primary buses, namely bus 1, 2 and 3. As expected, the angular frequency reduces as the load increases, and the rate of this decrease is affected by the inertia of the areas. Fig. 8(b) depicts the active power measurements measured from the same buses.

Subsequently, these signals are analysed using the proposed method by means of WT in Section III. Fig. 8 parts (c) and (d) present the fine-scale wavelet coefficients associated with the angular frequency and active power across the three areas,

TABLE II. System Parameters.

| Parameter | Definition | Value |
|---|---|---|
| $P_n^{G1}$ | Nominal power for generator 1 | 200 MW |
| $P_n^{GIC}$ | Nominal power for CIG | 200 MW |
| $P_n^{G2}$ | Nominal power for generator 2 | 200 MW |
| $\omega_n$ | Nominal grid frequency | 2π × 50 rad/s |
| $V_n$ | Nominal Grid voltage | 230 kV |
| $P_1, Q_1$ | Active and reactive power for load 1 | 140 MW, 30 MVAR |
| $P_2, Q_2$ | Active and reactive power for load 2 | 135 MW, 50 MVAR |
| $P_3, Q_3$ | Active and reactive power for load 3 | 100 MW, 35 MVAR |
| $H_{G1}, H_{G2}, H_{CIG}$ | Inertia constant for G1, G2 and CIG | 3.7 s |
| $D_{G1}, D_{G2}, D_{CIG}$ | Damping coefficients for G1, G2 and CIG | 0.05 pu, 0.05 pu, 20 pu |

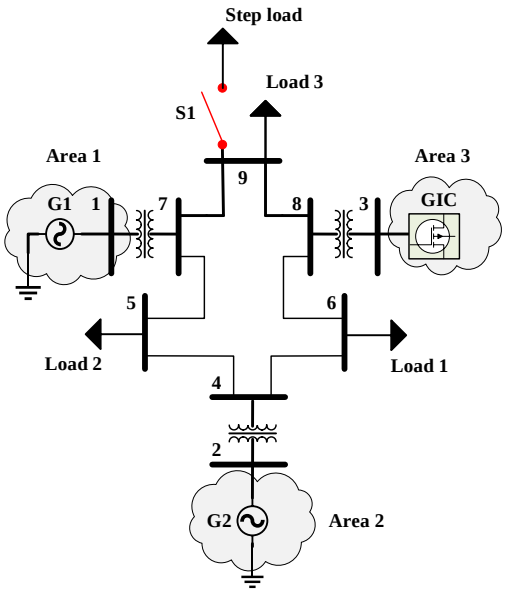


**Fig. 6.** IEEE 9 bus system.

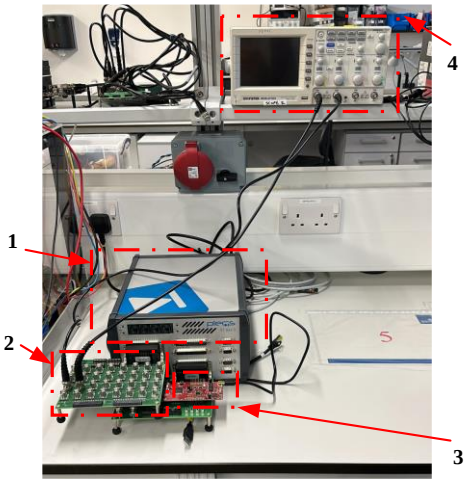


**Fig. 7.** Control hardware-in-the-loop validation. 1) PLECS RT simulator, 2) Box breakout board (for input/output interface), 3) DSP, and 4) Oscilloscope.

TABLE III. Transient Strength for Active Power and Frequency With Corresponding Equivalent Inertia Derived from Frequency Domain for Case Study 1.

| Transient strength | | Estimated inertia $(\frac{S_p^k}{S_\omega^k} \times \frac{2(\Delta t)^2}{\pi})$ | Actual inertia $(H_t^i)$ | Relative error (%) |
|---|---|---|---|---|
| $S_p^1$ | 9.1E-03 | 3.761 | 3.7 | 1.64% |
| $S_\omega^1$ | 1.54E-07 | | | |
| $S_p^2$ | 2.89E-03 | 3.889 | 3.7 | 5.11% |
| $S_\omega^2$ | 4.73E-08 | | | |
| $S_p^3$ | 3.1E-03 | 3.773 | 3.7 | 1.97% |
| $S_\omega^3$ | 5.23E-08 | | | |

respectively. The significant spike in the wavelet coefficient magnitude at 0.1 s indicates a transient event. The transient strength is determined by averaging five points around the peak value including the peak itself as described in the method in Section III. Table III presents the estimated inertia from the frequency domain across three areas in case study 1. Moreover, it shows the results of the proposed method in allocating the transient strengths for active power ($S_p^1$, $S_p^2$,$S_p^3$) and angular frequency ($S_\omega^1$,$S_\omega^2$,$S_\omega^3$). The estimated inertia is determined using the formula ($\frac{S_p^k}{S_\omega^k} \times \frac{2(\Delta t)^2}{\pi}$), where $\Delta t$ represents the transient the period, which has a value of 0.01. This transient period can be identified from any corresponding wavelet curve in Fig. 8(c) or Fig 8(d). Moreover, the table shows the actual inertia values for each area ($H_t^1$,$H_t^2$,$H_t^3$) and provides the relative error between the estimated value and the actual value. Generally, the errors are relatively small, demonstrating the accuracy of the estimation process. Notably, Area 2 exhibits a more significant relative error of 5.11%. This can be attributed to the fact that the transient load occurs at a location distant from Area 2, resulting in a minimal impact on the area transient characteristics, which in turn affects the accuracy of the inertia estimation in that area.

### *B. Case Study 2*

This case study assumes that the three areas have different inertia values: 10 s for G1 and 3.7 s for both CIG and G2. The study aims to validate whether the proposed method can recognise these variances or not. Furthermore, the measured

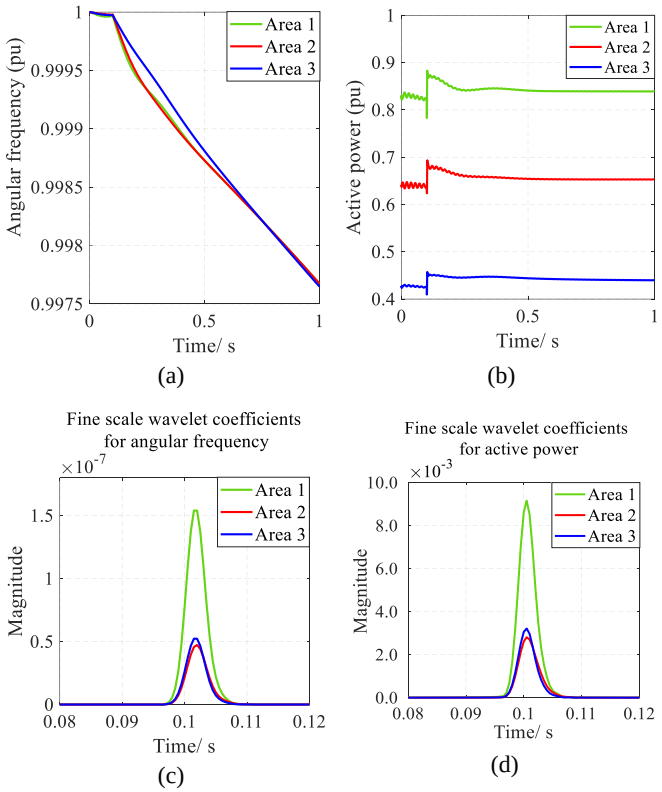


**Fig. 8.** Wavelet analysis for case study 1 consists of three areas with uniform inertia values: (a) Angular frequency responses, (b) active power responses, (c) fine scale wavelet coefficients for angular frequency signals, and (d) fine scale wavelet coefficients for active powers.

TABLE IV. TRANSIENTS' STRENGTH FOR ACTIVE POWER AND FREQUENCY WITH CORRESPONDING EQUIVALENT INERTIA DERIVED FROM FREQUENCY DOMAIN FOR CASE STUDY 2.

| Transients' strength | | Estimated inertia ($\frac{S_p^k}{S_\omega^k} \times \frac{2(\Delta t)^2}{\pi}$) | Actual inertia ($H_t^i$) | Relative error (%) |
|---|---|---|---|---|
| $S_p^1$ | 8.77E-03 | 10.188 | 10 | 1.88% |
| $S_\omega^1$ | 5.48E-08 | | | |
| $S_p^2$ | 3.23E-03 | 3.924 | 3.7 | 6.05% |
| $S_\omega^2$ | 5.24E-08 | | | |
| $S_p^3$ | 3.98E-03 | 3.781 | 3.7 | 2.18% |
| $S_\omega^3$ | 6.70E-08 | | | |

signals from PMUs are exposed to Gaussian white noise with a signal-to-noise ratio of 60 dB. This ratio is commonly observed in synchro-phasor measurements taken from transmission and distribution levels. The objective is to confirm the efficiency of the proposed method in the presence of such noise. Again, the transient event is triggered by applying a 40 MW load to bus 9 at 0.1s. Fig. 9 describes the results for case study 2. Fig 9(a) shows the angular frequency data from the main buses of each area, namely bus 1, 2 and 3. Since area 1 has the highest inertia, its angular frequency decreases at a slower rate. Fig. 9(b) illustrates how each of the three generators handles the extra power from the added load. Furthermore, the Gaussian white noise influence on the measured signals can be observed in Fig. 9 parts (a) and (b) in form of high frequency notches. The measured signals are then analysed using the proposed method in Section III. Fig. 9 parts (c) and (d) describe the fine-scale wavelet coefficients associated with the angular frequency and active power across the three areas, respectively. Again, the noticeable change in the wavelet data at 0.1 s suggests a transient event at that point. The increased inertia of area 1 in case study 2 is notably reflected in the frequency wavelet response. This is evidenced by the reduced strength of $S_f^1$ in case study 2 compared to its counterpart in case study 1. Table IV presents the estimated inertia in the frequency domain across the three areas of case study 2. The transient strengths for active power ($S_p^1$, $S_p^2$,$S_p^3$) and angular frequency ($S_\omega^1$, $S_\omega^2$,$S_\omega^3$) are determined using the proposed method. Moreover, the inertia constant is determined. Furthermore, the estimated inertia values are compared with the actual values and the relative errors are presented in Table IV. The relative errors are 1.88%, 6.05%, and 2.18% for area 1, area 2, and area 3, respectively. These errors are relatively small, which demonstrates the accuracy of the proposed method even with the noise from the PMUs.

### *C.* Comparative Analysis

A comparison of the proposed inertia estimation method with two other methods highlighted in recent research is conducted, using the same conditions from case study 2. This comparison aims to evaluate how accurately and consistently each method can estimate the inertia of G1 against the common noise issues in power system operations. Fig. 10 shows the estimated inertia for G1 using the three different methods: the fast response estimation method (FREM), the enhanced stability estimation method (ESEM) [6], and the proposed method. The FREM (estimates the inertia using (4)), noted for its quick response within 40 ms, shows significant deviations from the actual inertia value, highlighting its low numerical stability and noise resistance, with an unbounded steady-state error percentage.

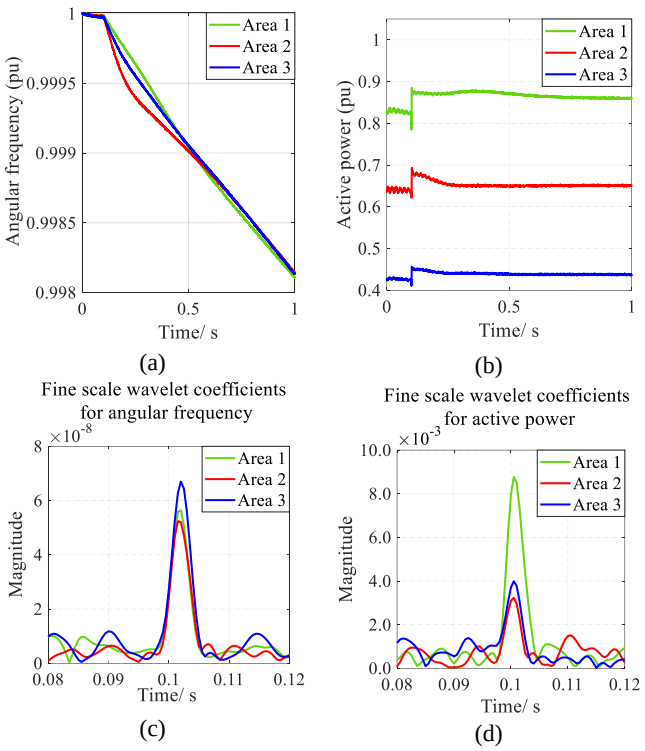


**Fig. 9.** Wavelet analysis for case study 2 consists of three areas with different inertia values. (a) Angular frequency responses, (b) active power responses, (c) fine scale wavelet coefficients for angular frequency signals., and (d) fine scale wavelet coefficients for active powers.

The ESEM, though slower with a response time within 200 ms, exhibits high numerical stability as indicated by the bounded steady-state error of ±10%. However, its noise resistance is low as it deviates from the actual value, particularly in the presence of noise. In contrast, the proposed method demonstrates a very fast response time of within 20 ms, coupled with high numerical stability and noise resistance. The proposed method closely follows the actual value, with minimal deviations. Its bounded steady-state error percentage is 1.88%, the lowest among the methods, indicating its superior performance in accurately estimating inertia in noisy conditions. Table V summarizes the comparison results.

## V. Sensitivity Analysis

As articulated in equations (2) and (5), the damping effect is not included. This assumption is predicated on the rapid responsiveness of the proposed estimation method, which operates within a critical 20 ms timeframe post-disturbance. During this period, the system response is predominantly governed by inertia, with damping effects considered to be minimal. This assumption holds under the typical values of the damping coefficient as mentioned in [21]. This subsection undertakes a sensitivity analysis on the damping coefficients This analysis is instrumental in defining the minimal effect condition for the damping coefficient, which delineates the operational boundaries within, which the proposed method maintains its efficacy and superiority.

The transient response of the system, as modelled by the swing equation in the time domain, is given by:

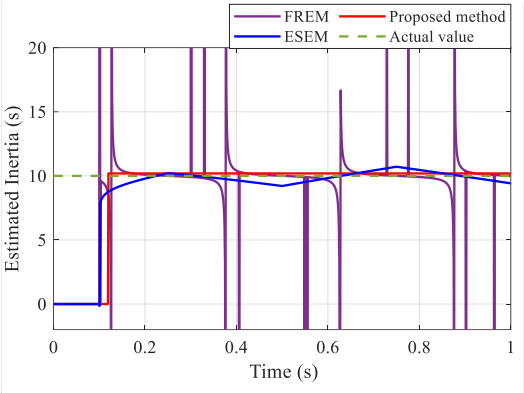


**Fig. 10** Comparative analysis of inertia estimation methods: FREM and ESEM vs. proposed method in noisy power system networks.

$$\omega_r(t) = \frac{\Delta P}{2H}\left(e^{-\frac{D}{2H}t}\right) \tag{20}$$

where, $D$ is the damping coefficient. For notably small values of $t$ during the initial transient response phase, the small-angle approximation for the exponential function can be employed ($e^{-x} \approx 1 - x$). This approximation underscores that for small $t$ (20 ms), the response is predominantly influenced by inertia $H$ with minimal contribution from damping as described below:

$$\omega_r(t)_{t\to 0} \approx \frac{\Delta P}{2H} \tag{21}$$

To quantitatively ascertain the minimal effect condition for damping, it is imperative that within the crucial 20 ms operational timeframe, the damping term should not significantly influence the system response. Employing a small-angle approximation for the exponential function provides:

$$e^{-\frac{D}{2H}\times 0.02} \approx 1 - \frac{D}{2H} \times 0.02 \tag{22}$$

In this formula the contribution of the $\frac{D}{2H} \times 0.02$ term should be much less than 1 for the damping be neglectable, then this simplifies to:

$$D \ll 100H \tag{23}$$

Therefore, it is crucial that $D$ remains much lower than $100H$ to minimize the impact of damping on the estimation method. This configuration ensures accurate detection of inertia within the initial 20 ms without substantial interference from damping. It is worth highlighting that this constraint aligns with the typical values for conventional synchronous machines and CIG designs, making the proposed estimation method reliable and compatible with the practical applications. Finally, for optimal results in complex interconnected systems, measurements should be conducted as proximally as possible to the area of interest, whether near synchronous machines or CIGs. This

TABLE V. Comparative Analysis of Inertia Estimation Methods.

| Method | Estimation Speed | Numerical Stability | Noise Resistance | Steady State error |
|---|---|---|---|---|
| FREM | Fast (40 ms) | Low | Low | Not bounded |
| ESEM | Slow (200 ms) | High | Low | ±10% |
| Proposed method | Very fast (20 ms) | High | High | 1.88% |

strategic positioning minimises the impact of noise and complex interactions. For example, in the IEEE 9-bus system, which comprises three areas, measurements are strategically taken from the buses directly connected to the area, such as bus 1, bus 2, and bus 3, as illustrated in Fig. 6.

## VI. Conclusion

This paper proposed an efficient, and reliable method to accurately estimate system inertia within the frequency domain for future power systems. The proposed method utilised the wavelet transform superior capability to identify and measure transients in measured power signals. The proposed method has unique advantages including its adaptability for real-time applications, computational efficiency, simplicity, and its ability to handle noisy signals. Moreover, this paper provided the mathematical derivation to find the relation between the inertia index estimated in the frequency domain and the actual inertia constant in the time domain. The proposed method is adaptable for both synchronous and non- synchronous power electronics-based converters. The proposed method was validated using control hardware-in-the-loop results in the PLECS for IEEE 9-bus system. The results demonstrated the superiority of this method in estimating inertia. In non-noisy signal conditions, the proposed inertia estimation method exhibits high precision in estimating inertia, with a maximum relative error of 5.1 %. Conversely, in noisy signal conditions, it maintains effectiveness, evidenced by a highest inertia estimation error of 6 %. These outcomes confirm the method robustness and accuracy in inertia estimation even in noisy conditions.

## Acknowledgement

This work was funded by the Energy Technology Partnership (ETP) and Scottish Power.

## References

[1] M. Dreidy, H. Mokhlis, and S. Mekhilef, "Inertia response and frequency control techniques for renewable energy sources: A review," *Renewable and sustainable energy reviews*, vol. 69, pp. 144-155, 2017.

[2] F. Milano, F. Dörfler, G. Hug, D. J. Hill, and G. Verbič, "Foundations and challenges of low-inertia systems," in *2018 power systems computation conference (PSCC)*, 2018: IEEE, pp. 1-25.

[3] P. Hu, Y. Li, Y. Yu, and F. Blaabjerg, "Inertia estimation of renewable-energy-dominated power system," *Renewable and Sustainable Energy Reviews*, vol. 183, p. 113481, 2023.

[4] K. Prabhakar, S. K. Jain, and P. K. Padhy, "Inertia estimation in modern power system: A comprehensive review," *Electric Power Systems Research*, vol. 211, p. 108222, 2022.

[5] B. Tan, J. Zhao, M. Netto, V. Krishnan, V. Terzija, and Y. Zhang, "Power system inertia estimation: Review of methods and the impacts of converter-interfaced generations," *International Journal of Electrical Power & Energy Systems*, vol. 134, p. 107362, 2022.

[6] M. Liu, J. Chen, and F. Milano, "On-line inertia estimation for synchronous and non-synchronous devices," *IEEE Transactions on Power Systems*, vol. 36, no. 3, pp. 2693-2701, 2020.

[7] H. Yin *et al.*, "Precise ROCOF estimation algorithm for low inertia power grids," *Electric Power Systems Research*, vol. 209, p. 107968, 2022.

[8] Y.-K. Wu, K. Le, T.-A. Nguyen, and O.-D. Phan, "Estimation of power system inertia using traditional swing equation, polynomial approximation and rv methods," in *2020 International Symposium on Computer, Consumer and Control (IS3C)*, 2020: IEEE, pp. 347-350.

[9] P. Wall and V. Terzija, "Simultaneous estimation of the time of disturbance and inertia in power systems," *IEEE Transactions on Power Delivery*, vol. 29, no. 4, pp. 2018-2031, 2014.

[10] E. R. Paidi, H. Marzooghi, J. Yu, and V. Terzija, "Development and validation of artificial neural network-based tools for forecasting of power system inertia with wind farms penetration," *IEEE Systems Journal*, vol. 14, no. 4, pp. 4978-4989, 2020.

[11] S. L. Brunton, J. L. Proctor, and J. N. Kutz, "Discovering governing equations from data by sparse identification of nonlinear dynamical systems," *Proceedings of the national academy of sciences*, vol. 113, no. 15, pp. 3932-3937, 2016.

[12] S. Lakshminarayana, S. Sthapit, and C. Maple, "A Comparison of Data-Driven Techniques for Power Grid Parameter Estimation," *arXiv preprint arXiv:2107.03762*, 2021.

[13] A. Hamid, D. Rafiq, S. A. Nahvi, and M. A. Bazaz, "Power Grid parameter estimation using Sparse Identification of Nonlinear Dynamics," in *2022 International Conference on Intelligent Controller and Computing for Smart Power (ICICCSP)*, 2022: IEEE, pp. 1-6.

[14] L. Lugnani, D. Dotta, C. Lackner, and J. Chow, "ARMAX-based method for inertial constant estimation of generation units using synchrophasors," *Electric Power Systems Research*, vol. 180, p. 106097, 2020.

[15] L. Fan and Y. Wehbe, "Extended Kalman filtering based real-time dynamic state and parameter estimation using PMU data," *Electric Power Systems Research*, vol. 103, pp. 168-177, 2013.

[16] A. K. Singh and B. C. Pal, "Rate of change of frequency estimation for power systems using interpolated DFT and Kalman filter," *IEEE Transactions on Power Systems*, vol. 34, no. 4, pp. 2509-2517, 2019.

[17] A. Rafinia and J. Moshtagh, "A new approach to fault location in three-phase underground distribution system using combination of wavelet analysis with ANN and FLS," *International Journal of Electrical Power & Energy Systems*, vol. 55, pp. 261-274, 2014.

[18] A. Bruce, D. Donoho, and H.-Y. Gao, "Wavelet analysis [for signal processing]," *IEEE spectrum*, vol. 33, no. 10, pp. 26-35, 1996.

[19] P. Kundur, "Power system stability," *Power system stability and control*, vol. 10, pp. 7-1, 2007.

[20] M. Farge, "Wavelet transforms and their applications to turbulence," *Annual review of fluid mechanics*, vol. 24, no. 1, pp. 395-458, 1992.

[21] P. S. Kundur and O. P. Malik, *Power system stability and control*. McGraw-Hill Education, 2022.

**MOHAMED ABOUYEHIA** received the B.Sc. degree in Electrical Engineering from Alexandria University, Alexandria, Egypt, in 2016, and the M.Sc. degree in Applied Mathematics from the Mathematics and Applied Physics Department, Alexandria University, Alexandria, Egypt, in 2021. He is an Assistant Lecturer with the Mathematics and Applied Physics Department, Faculty of Engineering, Alexandria University. He is currently pursuing the PhD degree at the University of Strathclyde, Glasgow, UK. His current research interests include renewable energy, smart grids, power system control.

**Agustí Egea-Àlvarez** (Member, IEEE) received the B.Sc., M.Sc., and Ph.D. degrees from the Technical University of Catalonia, Barcelona, in 2008, 2010, and 2014, respectively. In 2015, he was a Marie Curie Fellow with China Electric Power Research Institute (CEPRI). In 2016, he joined Siemens Gamesa Renewable Energy as a Converter Control Engineer, working on grid-forming controllers and alternative HVDC schemes for offshore wind farms. He is currently a Professor with the Electronic and Electrical Engineering Department and a member with the Power Electronics, Drives and Energy Conversion (PEDEC) Group. Also, he is the Holder of the Royal Academy of Engineering Industrial Fellowship, ScottishPower. He is a member of IET and has been involved in several CIGRE working groups.

**Sumeet S. Aphale** (Senior Member, IEEE) was a Professor and the Director of the Artificial Intelligence, Robotics, and Mechatronic Systems Group with the School of Engineering, University of Aberdeen, Aberdeen, U.K. His research work has been authored in more than 110 peer-reviewed journal and conference publications, showcasing the depth and breadth of his work. With career spanning nearly two decades, he has focused his research on the system-level design, analysis, instrumentation, control, and experimental validation of robotic and mechatronic systems. Which also includes subsea actuators, biomedical devices, renewable energy solutions, as well as sensing, and precision actuation technologies.
Prof. Aphale was the recipient of the best paper awards and nominations at several prestigious conferences for his research works. In recognition of his standing in the academic community, he has been an Associate Editor for IEEE Control Systems Letters and Frontiers of Mechanical Engineering (Mechatronics).

**Khaled H. Ahmed** (M'09–SM'12) received the B.Sc. (first class hons.) and M.Sc. degrees in electrical engineering from Alexandria University, Alexandria, Egypt, in 2002 and 2004, respectively. He received the Ph.D. degree in power electronics applications from the University of Strathclyde, Glasgow, UK, 2008. Currently, He is a Professor of Power Electronics at the University of Strathclyde, Glasgow, UK. He is a senior member of the IEEE Power Electronics and Industrial Electronics societies. He has published more than 185 technical papers in refereed journals and conferences as well as a published textbook entitled 'High Voltage Direct Current Transmission: Converters, Systems and DC Grids', a book chapter contribution, and a PCT patent PCT/GB2017/051364. Prof. Ahmed serves as a Co Editor-in-Chief of Elsevier Alexandria Engineering Journal, and as an Associate Editor of IEEE Open Journal of the Industrial Electronics Society (OJIES), and IEEE Access. His research interests are renewable energy integration, high power converters, offshore wind energy, DC/DC converters, HVDC, and smart grids.